Efficient Visible-Light-Driven Carbon Dioxide Reduction using a Bioinspired Nickel Molecular Catalyst

Jing Zhang, Ping She, Qiang Xu, Fengkun Tian, Heng Rao, Jun-sheng Qin, Julien Bonin, Marc Robert

ChemSusChem

Research Article
doi.org/10.1002/cssc.202301892

Chemistry Europe
European Chemical Societies Publishing

www.chemsuschem.org

Efficient Visible-Light-Driven Carbon Dioxide Reduction using a Bioinspired Nickel Molecular Catalyst

Jing Zhang[+],[a] Ping She[+],[a] Qiang Xu,[a] Fengkun Tian,[a] Heng Rao,*[a] Jun-Sheng Qin,*[a] Julien Bonin,[b] and Marc Robert*[b, c]

Inspired by natural enzymes, this study presents a nickel-based molecular catalyst, $[Ni^{II}(N_2S_2)]Cl_2$ (**NiN_2S_2**, N_2S_2 = 2,11-dithia[3,3](2,6)pyridinophane), for the photochemical catalytic reduction of CO_2 under visible light. The catalyst was synthesized and characterized using various techniques, including liquid chromatography-high resolution mass spectrometry (LC-HRMS), UV-Visible spectroscopy, and X-ray crystallography. The crystallographic analysis revealed a slightly distorted octahedral coordination geometry with a mononuclear Ni^{2+} cation, two nitrogen atoms and two sulfur atoms. Photocatalytic CO_2 reduction experiments were performed in homogeneous conditions using the catalyst in combination with $[Ru(bpy)_3]Cl_2$ (bpy = 2,2′-bipyridine) as a photosensitizer and 1,3-dimethyl-2-phenyl-2,3-dihydro-1*H*-benzo[*d*]imidazole (BIH) as a sacrificial electron donor. The catalyst achieved a high selectivity of 89% towards CO and a remarkable turnover number (TON) of 7991 during 8 h of visible light irradiation under CO_2 in the presence of phenol as a co-substrate. The turnover frequency (TOF) in the initial 6 h was 1079 h^{-1}, with an apparent quantum yield (AQY) of 1.08%. Controlled experiments confirmed the dependency on the catalyst, light, and sacrificial electron donor for the CO_2 reduction process. These findings demonstrate this bioinspired nickel molecular catalyst could be effective for fast and efficient photochemical catalytic reduction of CO_2 to CO.

Introduction

CO_2 resource exploitation has emerged as a significant way to contribute to "carbon neutrality" and to develop clean energy technology. In Nature, green plants employ chlorophyll to convert solar energy into chemical energy through photosynthesis while fixing CO_2 from the atmosphere to generate carbohydrates. They produce more than *ca.* 100 billion tons of biomass every year, which is equivalent to *ca.* 100 terawatts of stored energy. Therefore, converting solar energy into chemical energy and fixing CO_2 in the environment through artificial photosynthesis has emerged as a promising way to address energy issues.

CO_2 reduction is an energy demanding transformation for which catalysts are required.[1] Molecular catalysts mainly consist of metal-organic complexes which offer high atomic utilization efficiency, various structural modifications, high catalytic activity and selectivity. Additionally, molecular catalysts allow advanced spectroscopy analysis for multi-step reactions involving several electron transfers and intermediates during the reaction process. Homogeneous photocatalytic CO_2 reduction systems employing molecular catalysts have made significant progress in recent years. However, they often consist of noble metal centers, such as Re,[2] Ru,[3] and Ir,[4] which are rare and costly, preventing possible scale-up. Therefore, non-precious metal-based catalysts have attracted intense attention in recent years. They are widely used in catalysis research because they can both act as nucleophiles or electrophiles in chemical reactions, forming intermediates and lowering the activation energy. Recently, impressive results have been achieved with molecular catalysts based on Fe,[5] Co,[6] Ni[1d,7] or Cu[8] for CO_2 reduction. Among many examples, iron porphyrins with trifluoromethanesulfonic acid substituents exhibited good reduction activity and could selectively catalyze the reduction of CO_2 to CO with a turnover number (TON) of 5500.[5d] A water soluble cobalt porphyrin was reported to achieve a high CO_2 reduction activity with TON > 8000 in pure water system.[6d] A copper quaterpyridine catalyst showed even better photocatalytic activity for CO production, with a TON of 12400.[8a] In addition to CO, formic acid was also obtained as a 2-electron reduction product. For example, a Ni-based catalyst was recently reported with a TON of 14000 for formic acid.[1d] Most of the efficient non-noble metal molecular catalysts reported so far have improved stability due to their nitrogen atoms able to coordinate and stabilize metals, such as porphyrins[5e–n,6b–f,9] and phthalocyanines.[10] Other molecular catalysts have also used

[a] J. Zhang,[+] Dr. P. She,[+] Q. Xu, F. Tian, Prof. Dr. H. Rao, Prof. Dr. J.-S. Qin
State Key Laboratory of Inorganic Synthesis and Preparative Chemistry, College of Chemistry, International Center of Future Science, Jilin University, 2699 Qianjin Street, Changchun 130012, P. R. China
E-mail: rao@jlu.edu.cn
qin@jlu.edu.cn

[b] Prof. Dr. J. Bonin, Prof. Dr. M. Robert
Université Paris Cité, CNRS, Laboratoire d'Electrochimie Moléculaire (LEM), F-75013 Paris, France
E-mail: robert@u-paris.fr

[c] Prof. Dr. M. Robert
Institut Universitaire de France (IUF), F-75005 Paris, France
E-mail: robert@u-paris.fr

[+] These authors contributed equally to this work.

Supporting information for this article is available on the WWW under https://doi.org/10.1002/cssc.202301892

phosphorus[3a,c,4c] or sulfur[1d,7b,e,f,11] heteroatoms to coordinate with transition metal centers for stabilizing the complexes.

Nickel is a versatile transition metal which possesses various oxidation states (+4, +3, +2, +1, and 0) and is widely employed in photocatalytic reactions.[12] In Nature, several classes of Ni-enzymes[13] have been identified, including hydrogenases, ureases, carbon monoxide dehydrogenase (CODH), methyl-coenzyme M reductase and superoxide dismutase. The ligands of these enzymes contain nitrogen or sulfur atoms, which are Lewis bases[14] capable of donating electrons to the metal through σ or π bonds. These electron-donating properties increase electron density of the reducing metal center while maintaining strong metal-ligand covalence. Inspired by these enzymes, various biomimetic nickel catalysts have recently been developed for the photocatalytic CO_2 production.[12a,15] However, catalysts containing thiol ligands for CO_2 reduction are scarce in the literature.[1d,7b,e,f,11] Recently, inspired by the CODH enzyme, two Ni(||) complexes with N_2S_2-type[7f] tetradentate ligand and N_3S_2-type[7e] pentadentate ligand, respectively, were reported to catalyze the reduction of CO_2 to CO with high selectivity albeit with low TONs as compared to the state-of-the-art catalysts reported so far.[7d,16]

Herein, we report a Ni-based molecular catalyst $[Ni^{II}(N_2S_2)]Cl_2$ (**NiN_2S_2**, N_2S_2 = 2,11-dithia[3,3](2,6)pyridinophane)[17] containing thiol and pyridine ligands for the photochemical catalytic CO_2 reduction in an acetonitrile (MeCN)/H_2O mixed solvent, using $[Ru(bpy)_3]Cl_2$ (bpy = 2,2′-bipyridine) as a photosensitizer and 1,3-dimethyl-2-phenyl-2,3-dihydro-1*H*-benzo[*d*]imidazole (BIH) as a sacrificial electron donor. This homogeneous system exhibits high activity and selectivity for CO_2 reduction under visible light irradiation, offering a new approach for designing metal complex photocatalysts.

Results and Discussion

The N_2S_2 ligand was synthesized with minor modifications according to the literature[18] and obtained with a high yield of 92% (Figures S1–S4). **NiN_2S_2** was synthesized by reacting N_2S_2 with one equivalent of $NiCl_2$ in CH_2Cl_2, with 63% yield. The characterization of **NiN_2S_2** was performed by liquid chromatography-high resolution mass spectrometry (LC-HRMS, Figure S6), UV-Visible spectroscopy (Figure S7) and X-ray crystallography (Table S1). Details of the synthesis and characterization are given in the Supporting Material.

As shown in Figure 1, **NiN_2S_2** presents a slightly distorted octahedral coordination geometry with a mononuclear Ni^{2+} cation, two sulfur atoms and two nitrogen atoms, as shown by the crystalline structure. The two sulfur atoms occupy the *trans* biaxial position and the two pyridine nitrogen atoms occupy the *cis* position on the equatorial plane. Two chloride ions equilibrate charges. The sulfur and nitrogen atoms in the N_2S_2 ligand coordinate with the nickel center, increasing its charge density and thus potentially promoting its CO_2 reduction reactivity. The Ni–N and Ni–S bond distances in **NiN_2S_2** (Table S2) are comparable to those of other similar complexes.[7e,f, 19] However, the Ni–S bond distances are longer

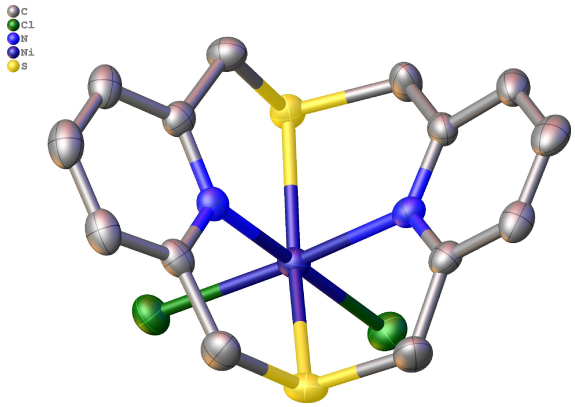

Figure 1. Crystallographic parameters of NiN_2S_2 from single-crystal X-ray diffraction. Element code: nickel (purple), carbon (grey), nitrogen (blue), sulphur (yellow) and chlorine (green). Hydrogen atoms are omitted for clarity.

than the Ni–N bond due to two factors. One is the larger size of the sulfur atom compared to the nitrogen atom, which leads to a more diffuse electron density and an extended bond length. The other is the weaker coordination bond between the sulfur lone pair and the metal *d* orbital as compared to the nitrogen lone pair and the metal *d* orbital, which lowers the bond strength. Moreover, the sulfur doping and the steric effects created by ligand distortion make the Ni–N bond distances in **NiN_2S_2** about 0.12 Å longer than in Ni(cyclam)$(ClO_4)_2$[20] and Ni-porphyrin.[21]

Photochemical CO_2 reduction was typically performed in a homemade quartz reactor containing a mixture of MeCN/H_2O (9.0 mL, v/v = 2:1), **NiN_2S_2** (1.0 μM), $[Ru(bpy)_3]Cl_2$ (0.7 mM) and BIH (0.02 M) saturated with CO_2. Figure 2 shows that during 72 h of visible light irradiation, 83 ± 3 μmol of CO was generated corresponding to a large TON of 9228 ± 321, with a turnover frequency (TOF) of 487 h^{-1} in the first 2 h and an apparent quantum yield (AQY) of 0.25%. Additionally, CO

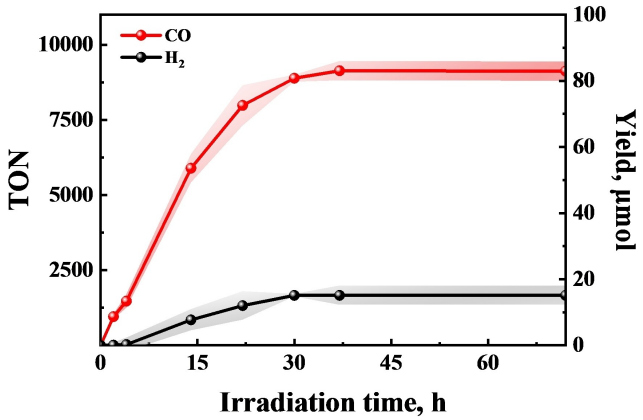

Figure 2. TON and yield (CO in red and H_2 in black) during visible light (420 nm) irradiation (72 h) of a MeCN/H_2O solution (9.0 mL, v/v = 2:1) containing **NiN_2S_2** (1.0 μM), $[Ru(bpy)_3]Cl_2$ (0.7 mM) and BIH (0.02 M) under CO_2 atmosphere. The error bands represent the standard error of the mean, which was determined from three runs.

selectivity was 85%. The main by-product was H_2 (15% selectivity) and trace amounts of formic acid were also detected in the liquid phase by ion chromatography (IC) analysis. Compared with other nickel-based homogeneous catalysts containing only Ni–N bonds (Table S3), this result illustrates that the introduction of Ni–S bonds significantly improves the performance of photocatalytic CO_2 reduction.

As illustrated in Figures 3 and S8, a series of control experiments were carried out to investigate how the various components affect the photocatalytic CO_2 reduction process. In the dark, no product was detected, confirming that the reaction is a light-driven process. A negligible amount of CO was observed without **NiN_2S_2** (probably due to $[Ru(bpy)_3]Cl_2$ low reactivity), indicating that the CO_2 reduction system requires **NiN_2S_2** to perform catalysis. Only H_2 was formed under Ar atmosphere, suggesting that CO_2 should be the sole source of CO. To further verify that CO_2 was the initial carbon source, we also performed experiments with $^{13}CO_2$ as the labelled reactant (Figure S9), and only ^{13}CO was generated in this experiment, further confirming that CO originated from CO_2. As illustrated in Figure 3, almost no CO was generated without $[Ru(bpy)_3]Cl_2$ or BIH, proving that both $[Ru(bpy)_3]Cl_2$ as a photosensitizer and BIH as a sacrificial electron donor are essential for the reaction. As Ru is a noble element, we tried a non-noble metal Cu-sensitizer [Cu(bathocuproine)(xantphos)](PF_6) (bathocuproine = 2,9-dimethyl-4,7-diphenyl-1,10-phenanthroline, xantphos = 4,5-bis(diphenylphosphino)-9,9-dimethylxanthene)[22] and an pure organic sensitizer 1,3-dicyano-2,4,5,6-tetrakis(N,N-diphenylamino)-benzene (4DPAIPN)[23] in the same system (Table 1). We also performed experiments with various sacrificial electron donors (triethylamine, TEA, and triethanolamine, TEOA, as shown in Table 1) and varying the concentration of BIH (Figure S10).

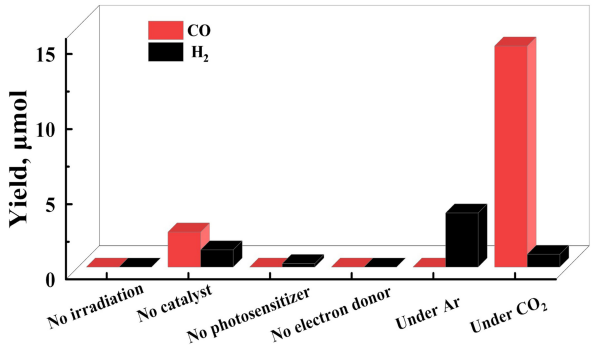

Figure 3. Yield obtained during control experiments (6 h irradiation) with either no light, no catalyst, no photosensitizer, no electron donor or under Ar atmosphere compared to the complete system.

According to our results, the optimal combination was $[Ru(bpy)_3]Cl_2$ and 0.02 M BIH. We further studied the effect of the concentration of **NiN_2S_2** (Figure S11) and observed that the yield of CO increases proportionally with increasing concentration of **NiN_2S_2**, following a first-order dependence at low (< 1.0 μM) concentration. At higher catalyst concentration, the yield of CO increased slowly, thus showing the beginning of a saturation regime. This observation suggests that the reaction is, at higher concentration of catalyst, under the control of both CO_2 binding and protonation steps. To rule out the possible formation of metal nanoparticles (NPs) from the molecular catalyst degradation, we performed a mercury poison test by adding a drop of mercury (Figure S12). It exhibited no significant difference on the yield of CO, excluding NPs formation. Dynamic light scattering (DLS) experiments (Figure S13) further proved that the catalytic process is homogeneous.

Finally, we tested the addition of an acid as a co-substrate, so as to accelerate the reaction, since it is well established that acids can not only stabilize the adduct between the CO_2 and the active catalyst but also significantly boost the carbon-oxygen bond cleavage.[24] We used trifluoroethanol (TFE) and phenol (PhOH) (see entries 6–10, Table 1), which are stronger acids than water, and in both cases the production rate for CO was significantly enhanced without compromising the selectivity. As illustrated in Figure 4, phenol, the strongest acid used in the study, led to the production of 71.92 μmol of CO during 8 h irradiation, corresponding to a TON of 7991, a selectivity for CO of 89% and an apparent quantum yield of 1.08%. A remarkable turnover frequency of 1079 h^{-1} (0.30 s^{-1}) was obtained in the first 6 hours.

Table 1. CO yield and selectivity during the photochemical reduction of CO_2 under various conditions.[a)]

Entry	Photosensitizer	Electron donor	Acid	Products	n_{CO}, μmol	CO Selectivity, %
1	$[Ru(bpy)_3]Cl_2$	BIH	None	CO, H_2	14.72	95
2[b)]	$[Ru(bpy)_3]Cl_2$	TEA	None	CO, H_2	0.19	19
3[c)]	$[Ru(bpy)_3]Cl_2$	TEOA	None	CO, H_2	2.10	90
4	[Cu(bathocuproine)(xantphos)](PF_6)	BIH	None	CO, H_2	0.57	84
5	4DPAIPN	BIH	None	CO, H_2	0.06	7
6	$[Ru(bpy)_3]Cl_2$	BIH	0.1 M TFE	CO, H_2	25.61	79
7	$[Ru(bpy)_3]Cl_2$	BIH	0.2 M TFE	CO, H_2	35.62	86
8	$[Ru(bpy)_3]Cl_2$	BIH	0.1 M PhOH	CO, H_2	39.54	92
9	$[Ru(bpy)_3]Cl_2$	BIH	0.2 M PhOH	CO, H_2	58.28	89

a) Standard conditions: photosensitizer (0.7 mM), **NiN_2S_2** (1.0 μM), and BIH (0.02 M) in 9.0 mL CO_2-saturated solution under 420 nm LED irradiation for 6 h. b) [TEA] = 0.02 M. c) [TEOA] = 0.02 M.

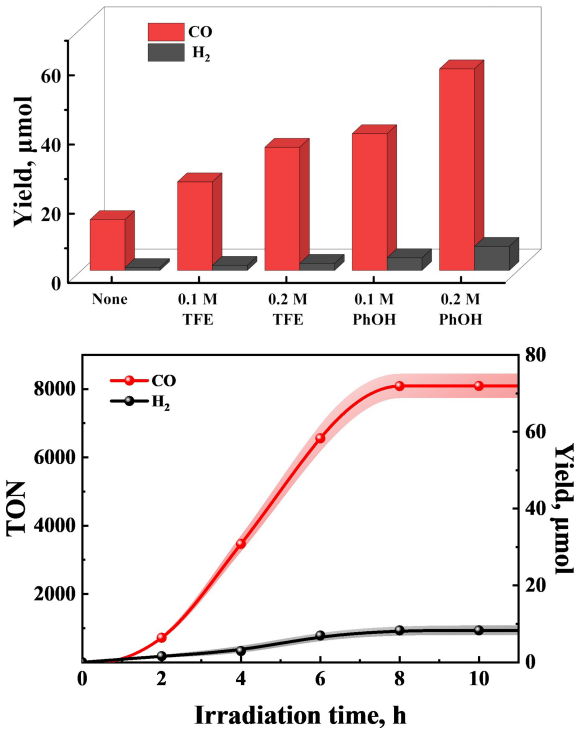

Figure 4. Irradiation with visible light (420 nm) of a MeCN/H_2O solution (9.0 mL, v/v = 2:1) containing **NiN_2S_2** (1.0 µM), $[Ru(bpy)_3]Cl_2$ (0.7 mM), BIH (0.02 M) and weak acid under CO_2 atmosphere. Top: Yield obtained (CO in red and H_2 in black) during a 6 h experiment. Bottom: TON and yield (CO in red and H_2 in black) in the presence of 0.2 M PhOH as a function of time. The error bands represent the standard error of the mean, which was determined from three runs.

Our data shows that **NiN_2S_2** exhibits high photocatalytic performance. However, the production of CO stops after 37 h of reaction. A series of experiments were thus conducted to analyze the possible limiting factors. After 37 h of irradiation, either initial concentration of **NiN_2S_2**, $[Ru(bpy)_3]Cl_2$ or BIH was re-added, respectively (Figure S14). The activity of the photocatalytic system was partially recovered after the addition of $[Ru(bpy)_3]Cl_2$ or BIH, and it reached a plateau in 7 h. Since one BIH molecule provides two electrons to form BI^+,[25] enough for the formation of CO or H_2, the initial BIH is slightly in excess. Similar results could also be observed when we re-added both BIH and **NiN_2S_2**. However, the catalytic activity was significantly recovered after re-adding both BIH and $[Ru(bpy)_3]Cl_2$, showing that the photosensitizer $[Ru(bpy)_3]Cl_2$ and sacrificial electron donor BIH present a limited stability whereas catalyst **NiN_2S_2** seems to be highly stable, even under prolonged irradiation.

In order to investigate the mechanism of CO_2 reduction by **NiN_2S_2**, we conducted cyclic voltammetry (CV) measurements with a glassy carbon (GC) working electrode, a Pt wire counter electrode and a saturated calomel electrode (SCE) reference electrode. Two reduction waves at −1.28 V and −1.58 V *vs.* SCE were observed under Ar atmosphere (Figures S15–16), which were assigned to the $Ni^{II/I}$ and $Ni^{I/0}$ one-electron reduction processes, respectively. These waves very likely coincide with the concomitant loss of the chloride anions. Under CO_2 atmosphere, the catalytic activity starts at the first reduction with a marked increase in current. The photocatalytic reaction mechanism was further explored by UV-Visible spectroscopy under Xe lamp irradiation. Individual UV-visible spectra of the **NiN_2S_2**, $[Ru(bpy)_3]Cl_2$ and BIH are shown in Figures S7 and S17, respectively. In Figure 5a–b, under Ar or CO_2 atmosphere in the absence of $[Ru(bpy)_3]Cl_2$, we observed no significant change in the absorption spectrum. In Figure 5c, with the full system (catalyst, photosensitizer and sacrificial electron donor) under Ar atmosphere, no change in the absorption spectrum was observed as well. On the contrary, under CO_2 atmosphere, the absorbance of $[Ru(bpy)_3]Cl_2$ and BIH gradually decreased (Figure 5d), suggesting that electron transfer occurred in the three-component system under CO_2 atmosphere.

To elucidate the electron transfer pathway in the photochemical process, we performed emission quenching experiments and luminescence lifetime experiments. The steady-state photoluminescence (PL) intensity for $[Ru(bpy)_3]Cl_2$ was efficiently quenched by BIH but not quenched by **NiN_2S_2**, indicating a reductive quenching pathway in the photochemical catalytic process (Figure S18). According to the Stern-Volmer analysis, the reductive quenching rate constant of $*3[Ru^{II}(bpy)_3]^{2+}$ by BIH is $2.9\times10^9\ M^{-1}s^{-1}$. The luminescence lifetime (Figure S19) of $*3[Ru^{II}(bpy)_3]^{2+}$ (219.6 ± 0.4 ns) was not modified with the addition of **NiN_2S_2** (222.5 ± 0.4 ns). However, it decreased to 112.2 ± 0.3 ns with the addition of BIH, further demonstrating a reductive quenching pathway is followed in the photochemical catalytic process.

The nanosecond transient absorption spectra of the photocatalytic system were measured to further elucidate the electron transfer dynamics (Figure 6, Figures S20–22). In Figure 6a–d, after laser excitation at 355 nm, a positive absorption band of the excited state $*3[Ru^{II}(bpy)_3]^{2+}$ appeared at 365 nm and a negative bleaching band of the ground state $[Ru^{II}(bpy)_3]^{2+}$ appeared at 447 nm,[26] respectively. The addition of **NiN_2S_2** did not affect the absorption signal (Figure 6b). However, a new absorption band emerged at 510 nm[27] with the addition of BIH (Figure 6c), indicating the $*3[Ru^{II}(bpy)_3]^{2+}$ was reductively quenched by BIH to form the $[Ru^{I}(bpy)_3]^{+}$. In Figure 6d–f, the addition of **NiN_2S_2** reduced the signal growth of $[Ru^{I}(bpy)_3]^{+}$ from 96 ns to 65 ns and reduced the signal decay of $[Ru^{I}(bpy)_3]^{+}$ from 199 ns to 144 ns. This finding shows that **NiN_2S_2** plays a key role in the formation and conversion of $[Ru^{I}(bpy)_3]^{+}$, which is capable of efficiently transfer electrons to **NiN_2S_2** for the subsequent catalytic reaction.

Based on all the above data, we propose the following reaction mechanism (Scheme 1). Upon light excitation, $[Ru(bpy)_3]^{2+}$ photosensitizer is promoted to its triplet metal-to-ligand charge transfer (MLCT) excited state $*3[Ru^{II}(bpy)_3]^{2+}$. The latter is reductively quenched by BIH to generate $[Ru^{I}(bpy)_3]^{+}$ and the one electron oxidized species $BIH^{\bullet+}$ may quickly deprotonate to give a very strong electron donor $BI^{\bullet}$ (E_{ox} = −2.06 V *vs.* Fc^+/Fc).[28] $[Ru^{I}(bpy)_3]^{+}$ transfers an electron to $[Ni^{II}N_2S_2]^{2+}$ to form the reactive $[Ni^{I}N_2S_2]^{+}$ species, which will combine CO_2 to form $[Ni^{I}N_2S_2\text{-}CO_2]^{+}$ intermediate. $[Ni^{I}N_2S_2\text{-}CO_2]^{+}$ further obtains an electron from $BI^{\bullet}$ to form $[Ni^{0}N_2S_2\text{-}CO_2]$ species. Finally, $[Ni^{0}N_2S_2\text{-}CO_2]$ led to CO formation from protonation of the adduct and O–H bond cleavage, and returns

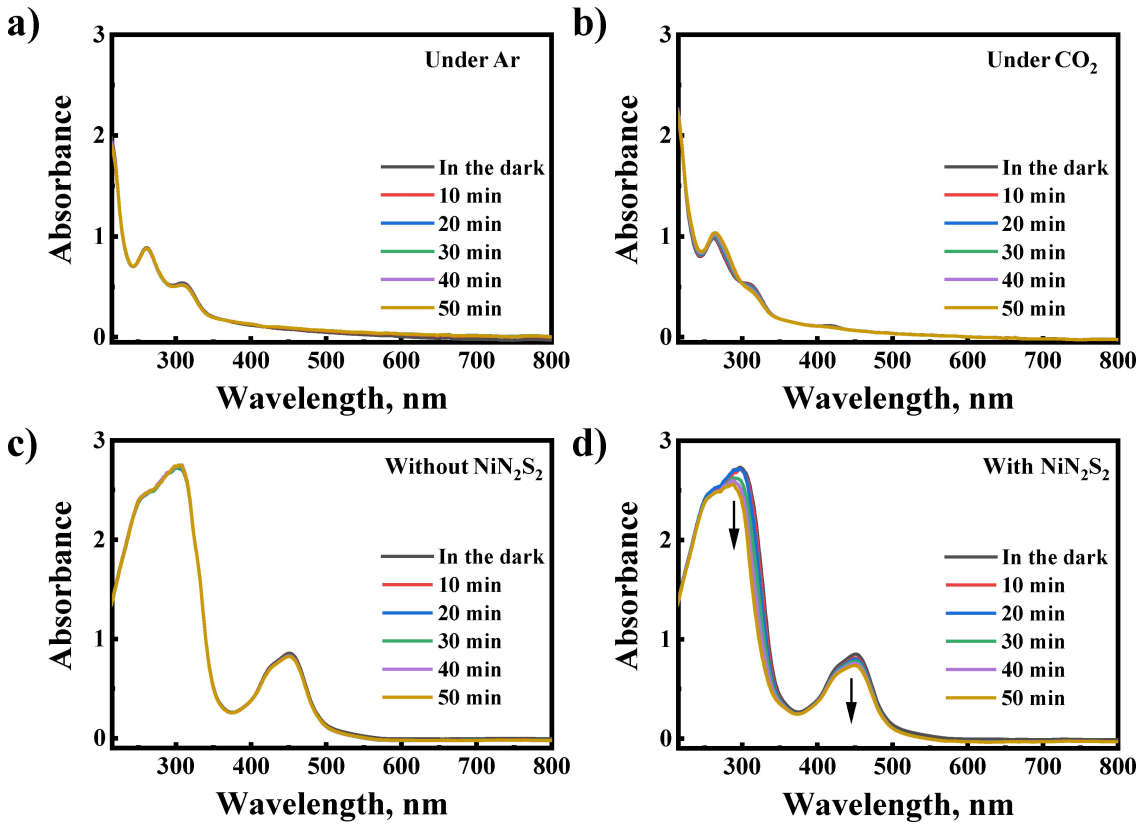

Figure 5. UV-Visible spectral changes upon irradiation of a MeCN/H_2O (3.0 mL, v/v = 2:1) solution containing **NiN_2S_2** (30 μM) and BIH (50 μM) a) under Ar atmosphere and b) under CO_2 atmosphere. c) UV-Visible spectral changes upon irradiation of a CO_2-saturated MeCN/H_2O (3.0 mL, v/v = 2:1) solution containing **NiN_2S_2** (0.1 μM), $[Ru(bpy)_3]Cl_2$ (70 μM) and BIH (2.0 mM). d) Without **NiN_2S_2**. T = 298 K, using Xe lamp irradiation (with a λ = 420 nm cut-off filter, 179 mW cm^{-2}).

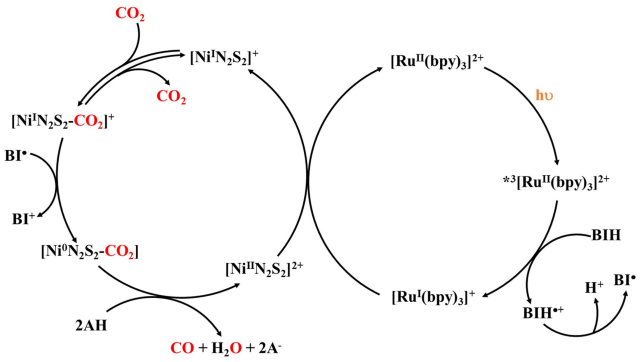

Scheme 1. Proposed mechanism for the CO_2 photochemical catalytic conversion to CO by catalyst **NiN_2S_2** combined with $[Ru(bpy)_3]Cl_2$ photosensitizer, and BIH sacrificial electron donor upon visible light irradiation.

to the $[Ni^{II}N_2S_2]^{2+}$ state (possibly after a dissociation step to release a bound CO), accomplishing a catalytic cycle. Our results suggest that the rate-determining step (RDS) for CO_2 reduction by **NiN_2S_2** may be the CO_2 coordination to the reduced $[Ni^{I}N_2S_2]^+$ species, although further *operando* characterization is required to investigate the intermediate derived from **NiN_2S_2**.

Conclusions

In summary, we have developed an efficient photocatalytic CO_2 reduction system using homogeneous catalyst **NiN_2S_2**, bearing a sulfur-containing macrocyclic ligand inspired by the CODH enzyme to produce CO selectively in the presence of $[Ru(bpy)_3]^{2+}$ as photosensitizer and BIH as electron donor. High production rate, up to 10^3 h^{-1}, was achieved with phenol as a co-substrate along with 89% selectivity for CO and a high turnover number (close to 8000) during 8 h of irradiation. These performances make the catalyst one of the most active in the photochemical catalytic CO_2 reduction to date. We are currently optimizing the coordination environments of the ligands to further investigate their effects on catalyst performance.

Supporting Information

Additional experimental details are given in the Supporting Information, including chemicals and catalyst preparation, instruments, ^1H and ^{13}C NMR spectra, LC-HRMS and GC-MS data, UV-Visible spectra, control and optimization experiments, DLS spectra, addition experiments, electrochemistry data, Stern-Volmer plot, luminescence lifetime and transient absorption

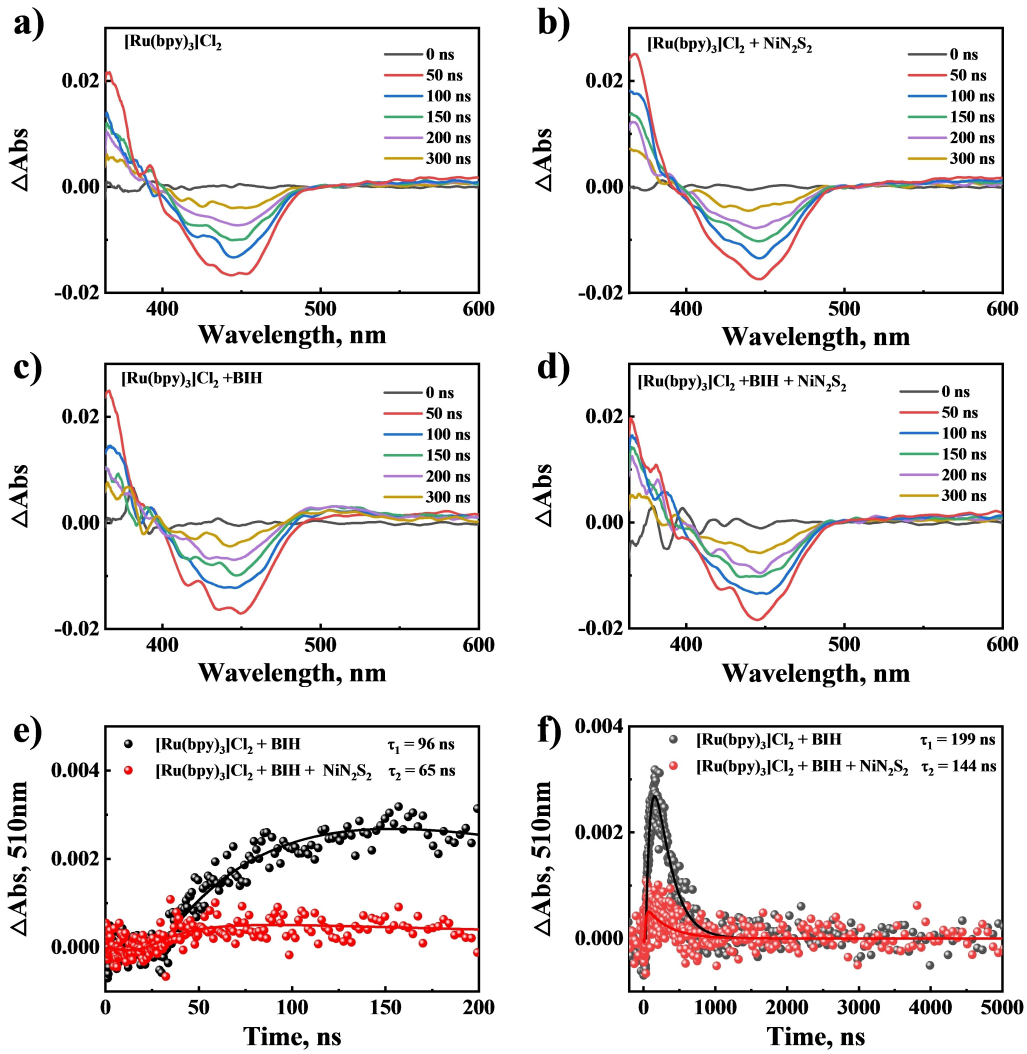

Figure 6. Transient absorption spectra following 355 nm laser excitation (pulse duration 1 ns, pulse energy 7 μJ, repetition rate 1 kHz) in MeCN/H_2O (v/v = 9:1) solution of **a)** 0.15 mM $[Ru(bpy)_3]Cl_2$ (0–300 ns after laser pulse excitation); **b)** 0.15 mM $[Ru(bpy)_3]Cl_2$ and 0.1 mM NiN_2S_2 (0–300 ns after laser pulse excitation); **c)** 0.15 mM $[Ru(bpy)_3]Cl_2$ and 1.0 mM BIH (0–300 ns after laser pulse excitation). **d)** 0.15 mM $[Ru(bpy)_3]Cl_2$, 1.0 mM BIH and 0.1 mM NiN_2S_2 (0–300 ns after laser pulse excitation). **e)** Kinetic analysis of the $[Ru^{I}(bpy)_3]^+$ signal growth probed at 510 nm without NiN_2S_2 (black trace) and with NiN_2S_2 (red trace). **f)** Kinetic analysis of the $[Ru^{I}(bpy)_3]^+$ signal decay probed at 510 nm without NiN_2S_2 (black trace) and with NiN_2S_2 (red trace).

spectra measurements, X-ray crystallographic data and comparison of catalytic activity with previous data from literature.

Additional references cited within the Supporting Information.[29–41]

Acknowledgements

This work was financially supported in part by the Natural Science Foundation of Jilin Province (No. SKL202302017), the National Natural Science Foundation of China (Grant Nos. 21901084, 21905106 and 22279041), the National Key Research and Development Program of China (No. 2022YFC2105800), the 111 Project (B17020), and the Specific Research Fund of the Innovation Platform for Academicians of Hainan Province, China (YSPTZX202321). Partial financial support to M.R. from the Institut Universitaire de France (IUF) is warmly thanked.

Conflict of Interests

The authors declare no conflict of interest.

Data Availability Statement

The data that support the findings of this study are available from the corresponding author upon reasonable request.

Keywords: molecular catalyst · CO_2 reduction · visible light · Nickel complex · homogeneous catalysis

[1] a) F. Guo, R. X. Li, S. Yang, X. Y. Zhang, H. Yu, J. J. Urban, W. Y. Sun, *Angew. Chem. Int. Ed.* **2023**, *62*, e202216232; b) M. Elcheikh Mahmoud, H. Audi, A. Assoud, T. H. Ghaddar, M. Hmadeh, *J. Am. Chem. Soc.* **2019**, *141*, 7115–7121; c) D. C. Liu, H. H. Huang, J. W. Wang, L.

Jiang, D. C. Zhong, T. B. Lu, *ChemCatChem* **2018**, *10*, 3435–3440; d) S. E. Lee, A. Nasirian, Y. E. Kim, P. T. Fard, Y. Kim, B. Jeong, S.-J. Kim, J.-O. Baeg, J. Kim, *J. Am. Chem. Soc.* **2020**, *142*, 19142–19149; e) M. Sun, C. Wang, C.-Y. Sun, M. Zhang, X.-L. Wang, Z.-M. Su, *J. Catal.* **2020**, *385*, 70–75.

[2] a) Y. Kou, Y. Nabetani, D. Masui, T. Shimada, S. Takagi, H. Tachibana, H. Inoue, *J. Am. Chem. Soc.* **2014**, *136*, 6021–6030; b) Y. Hameed, P. Berro, B. Gabidullin, D. Richeson, *Chem. Commun.* **2019**, *55*, 11041–11044; c) Y. Kuramochi, O. Ishitani, H. Ishida, *Coord. Chem. Rev.* **2018**, *373*, 333–356; d) B. M. Pirzada, A. H. Dar, M. N. Shaikh, A. Qurashi, *ACS Omega* **2021**, *6*, 29291–29324; e) A. Maurin, C.-O. Ng, L. Chen, T.-C. Lau, M. Robert, C.-C. Ko, *Dalton Trans.* **2016**, *45*, 14524–14529; f) N. Elgrishi, M. B. Chambers, X. Wang, M. Fontecave, *Chem. Soc. Rev.* **2017**, *46*, 761–796.

[3] a) S. K. Lee, M. Kondo, M. Okamura, T. Enomoto, G. Nakamura, S. Masaoka, *J. Am. Chem. Soc.* **2018**, *140*, 16899–16903; b) S. K. Lee, M. Kondo, G. Nakamura, M. Okamura, S. Masaoka, *Chem. Commun.* **2018**, *54*, 6915–6918; c) Y. Hameed, G. K. Rao, J. S. Ovens, B. Gabidullin, D. Richeson, *ChemSusChem* **2019**, *12*, 3453–3457; d) Y. Arikawa, I. Tabata, Y. Miura, H. Tajiri, Y. Seto, S. Horiuchi, E. Sakuda, K. Umakoshi, *Chem. Eur. J.* **2020**, *26*, 5603–5606; e) Y. Kuramochi, J. Itabashi, M. Toyama, H. Ishida, *ChemPhotoChem* **2018**, *2*, 314–322; f) Y. Kuramochi, K. Fukaya, M. Yoshida, H. Ishida, *Chem. Eur. J.* **2015**, *21*, 10049–10060; g) Y. Kuramochi, J. Itabashi, K. Fukaya, A. Enomoto, M. Yoshida, H. Ishida, *Chem. Sci.* **2015**, *6*, 3063–3074; h) H. Ishida, A. Sakaba, *Faraday Discuss.* **2017**, *198*, 263–277.

[4] a) K. Kamada, J. Jung, Y. Kametani, T. Wakabayashi, Y. Shiota, K. Yoshizawa, S. H. Bae, M. Muraki, M. Naruto, K. Sekizawa, S. Sato, T. Morikawa, S. Saito, *Chem. Commun.* **2022**, *58*, 9218–9221; b) S. Sato, T. Morikawa, *ChemPhotoChem* **2017**, *2*, 207–212; c) K. Kamada, J. Jung, T. Wakabayashi, K. Sekizawa, S. Sato, T. Morikawa, S. Fukuzumi, S. Saito, *J. Am. Chem. Soc.* **2020**, *142*, 10261–10266.

[5] a) M. Loipersberger, D. G. A. Cabral, D. B. K. Chu, M. Head-Gordon, *J. Am. Chem. Soc.* **2021**, *143*, 744–763; b) E. Boutin, L. Merakeb, B. Ma, B. Boudy, M. Wang, J. Bonin, E. Anxolabéhère-Mallart, M. Robert, *Chem. Soc. Rev.* **2020**, *49*, 5772–5809; c) L. Chen, G. Chen, C.-F. Leung, C. Cometto, M. Robert, T.-C. Lau, *Chem. Soc. Rev.* **2020**, *49*, 7271–7283; d) A. Stoumpidi, A. Trapali, M. Poisson, A. Barrozo, S. Bertaina, M. Orio, G. Charalambidis, A. G. Coutsolelos, *ChemCatChem* **2023**, *15*; e) H. Yuan, B. Cheng, J. Lei, L. Jiang, Z. Han, *Nat. Commun.* **2021**, *12*, 1835; f) J. Grodkowski, D. Behar, P. Neta, P. Hambright, *J. Phys. Chem. A* **1997**, *101*, 248–254; g) J. Bonin, M. Chaussemier, M. Robert, M. Routier, *ChemCatChem* **2014**, *6*, 3200–3207; h) J. Bonin, M. Robert, M. Routier, *J. Am. Chem. Soc.* **2014**, *136*, 16768–16771; i) H. Rao, J. Bonin, M. Robert, *Chem. Commun.* **2017**, *53*, 2830–2833; j) H. Rao, J. Bonin, M. Robert, *ChemSusChem* **2017**, *10*, 4447–4450; k) H. Rao, C.-H. Lim, J. Bonin, G. M. Miyake, M. Robert, *J. Am. Chem. Soc.* **2018**, *140*, 17830–17834; l) H. Rao, J. Bonin, M. Robert, *J. Phys. Chem. C* **2018**, *122*, 13834–13839; m) M. Kientz, G. Lowe, B. G. McCarthy, G. M. Miyake, J. Bonin, M. Robert, *ChemPhotoChem* **2022**, *6*; n) A. Dannenhoffer, H. Sai, D. Huang, B. Nagasing, B. Harutyunyan, D. J. Fairfield, T. Aytun, S. M. Chin, M. J. Bedzyk, M. Olvera de la Cruz, S. I. Stupp, *Chem. Sci.* **2019**, *10*, 5779–5786.

[6] a) T. Ouyang, H. H. Huang, J. W. Wang, D. C. Zhong, T. B. Lu, *Angew. Chem. Int. Ed.* **2016**, *56*, 738–743; b) A. Call, M. Cibian, K. Yamamoto, T. Nakazono, K. Yamauchi, K. Sakai, *ACS Catal.* **2019**, *9*, 4867–4874; c) X. Zhang, M. Cibian, A. Call, K. Yamauchi, K. Sakai, *ACS Catal.* **2019**, *9*, 11263–11273; d) F. Arcudi, L. Đorđević, B. Nagasing, S. I. Stupp, E. A. Weiss, *J. Am. Chem. Soc.* **2021**, *143*, 18131–18138; e) G. F. Manbeck, E. Fujita, *J. Porphyrins Phthalocyanines* **2015**, *19*, 45–64; f) X. Zhang, K. Yamauchi, K. Sakai, *ACS Catal.* **2021**, *11*, 10436–10449.

[7] a) D. B. Burks, S. Davis, R. W. Lamb, X. Liu, R. R. Rodrigues, N. P. Liyanage, Y. Sun, C. E. Webster, J. H. Delcamp, E. T. Papish, *Chem. Commun.* **2018**, *54*, 3819–3822; b) D. Hong, T. Kawanishi, Y. Tsukakoshi, H. Kotani, T. Ishizuka, T. Kojima, *J. Am. Chem. Soc.* **2019**, *141*, 20309–20317; c) J. Lin, B. Qin, Z. Fang, *Catal. Lett.* **2018**, *149*, 25–33; d) H. Shirley, X. Su, H. Sanjanwala, K. Talukdar, J. W. Jurss, J. H. Delcamp, *J. Am. Chem. Soc.* **2019**, *141*, 6617–6622; e) Q. He, B. Wu, Y. Hu, W. Huang, Y. Li, *Sci. China Chem.* **2020**, *63*, 1716–1720; f) D. Hong, Y. Tsukakoshi, H. Kotani, T. Ishizuka, T. Kojima, *J. Am. Chem. Soc.* **2017**, *139*, 6538–6541.

[8] a) Z. Guo, F. Yu, Y. Yang, C. F. Leung, S. M. Ng, C. C. Ko, C. Cometto, T. C. Lau, M. Robert, *ChemSusChem* **2017**, *10*, 4009–4013; b) J. Bian, L. Sun, Z. Zhang, Z. Li, M. Chu, X. Li, D. Tang, L. Jing, *ACS Sustainable Chem. Eng.* **2021**, *9*, 2400–2408; c) W. J. Liu, H. H. Huang, T. Ouyang, L. Jiang, D. C. Zhong, W. Zhang, T. B. Lu, *Chem. Eur. J.* **2018**, *24*, 4503–4508.

[9] H. Rao, L. C. Schmidt, J. Bonin, M. Robert, *Nature* **2017**, *548*, 74–77.

[10] a) J. Sun, J. Bian, J. Li, Z. Zhang, Z. Li, Y. Qu, L. Bai, Z.-D. Yang, L. Jing, *Applied Cat. B* **2020**, *277*, 119199; b) J. Bian, J. Feng, Z. Zhang, Z. Li, Y. Zhang, Y. Liu, S. Ali, Y. Qu, L. Bai, J. Xie, D. Tang, X. Li, F. Bai, J. Tang, L. Jing, *Angew. Chem. Int. Ed.* **2019**, *58*, 10873–10878; c) J. Bian, J. Feng, Z. Zhang, J. Sun, M. Chu, L. Sun, X. Li, D. Tang, L. Jing, *Chem. Commun.* **2020**, *56*, 4926–4929; d) B. Li, L. Sun, J. Bian, N. Sun, J. Sun, L. Chen, Z. Li, L. Jing, *Applied Cat. B* **2020**, *270*, 118849; e) W.-J. Ong, L.-L. Tan, Y. H. Ng, S.-T. Yong, S.-P. Chai, *Chem. Rev.* **2016**, *116*, 7159–7329; f) F. Franco, C. Rettenmaier, H. S. Jeon, B. Roldan Cuenya, *Chem. Soc. Rev.* **2020**, *49*, 6884–6946; g) S. Roy, E. Reisner, *Angew. Chem. Int. Ed.* **2019**, *58*, 12180–12184; h) G. Liu, Y. Wang, Y. Zhou, J. Cao, M. Yuan, H. Lv, *J. Colloid Interface Sci.* **2021**, *594*, 658–668; i) Y. Wang, Y. Zhu, L. Sun, F. Li, *ACS Appl. Mater. Interfaces* **2020**, *12*, 41644–41648.

[11] B. Zhang, S. Yang, X. Zheng, Y.-w. Ju, B.-Z. Chen, *Organometallics* **2020**, *39*, 1176–1186.

[12] a) T. Kojima, *ChemPhotoChem* **2021**, *5*, 512–520; b) L. Mantry, R. Maayuri, V. Kumar, P. Gandeepan, *Beilstein J. Org. Chem.* **2021**, *17*, 2209–2259; c) A. Mazzeo, S. Santalla, C. Gaviglio, F. Doctorovich, J. Pellegrino, *Inorg. Chim. Acta* **2021**, *517*, 119950; d) L. Tong, L. Duan, A. Zhou, R. P. Thummel, *Coord. Chem. Rev.* **2020**, *402*, 213079.

[13] a) M. A. Halcrow, G. Christou, *Chem. Rev.* **1994**, *94*, 2421–2481; b) C. P. Dai Yan, *Prog. Chem.* **2002**, *14*, 47–55.

[14] a) M. R. Koebel, A. Cooper, G. Schmadeke, S. Jeon, M. Narayan, S. Sirimulla, *J. Chem. Inf. Model.* **2016**, *56*, 2298–2309; b) S. Dey, T. K. Todorova, M. Fontecave, V. Mougel, *Angew. Chem. Int. Ed.* **2020**, *59*, 15726–15733.

[15] J.-W. Wang, W.-J. Liu, D.-C. Zhong, T.-B. Lu, *Coord. Chem. Rev.* **2019**, *378*, 237–261.

[16] V. S. Thoi, N. Kornienko, C. G. Margarit, P. Yang, C. J. Chang, *J. Am. Chem. Soc.* **2013**, *135*, 14413–14424.

[17] E. C. Constable, J. Lewis, V. E. Marquez, P. R. Raithby, *J. Chem. Soc. Dalton Trans.* **1986**, 1747–1749.

[18] T. Moriguchi, S. Kitamura, K. Sakata, A. Tsuge, *Polyhedron* **2001**, *20*, 2315–2320.

[19] P. Gotico, D. Moonshiram, C. Liu, X. Zhang, R. Guillot, A. Quaranta, Z. Halime, W. Leibl, A. Aukauloo, *Chem. Eur. J.* **2020**, *26*, 2859–2868.

[20] L. Prasad, S. C. Nyburg, A. McAuley, *Acta Crystallogr. Sect. C* **1987**, *43*, 1038–1042.

[21] A. E. Pogonin, A. A. Otlyotov, Y. Minenkov, A. S. Semeikin, Y. A. Zhabanov, S. A. Shlykov, G. V. Girichev, *Int. J. Mol. Sci.* **2021**, *23*, 320.

[22] Y. Sakaguchi, A. Call, M. Cibian, K. Yamauchi, K. Sakai, *Chem. Commun.* **2019**, *55*, 8552–8555.

[23] A. F. Chmiel, O. P. Williams, C. P. Chernowsky, C. S. Yeung, Z. K. Wickens, *J. Am. Chem. Soc.* **2021**, *143*, 10882–10889.

[24] a) B. Ma, M. Blanco, L. Calvillo, L. Chen, G. Chen, T.-C. Lau, G. Dražić, J. Bonin, M. Robert, G. Granozzi, *J. Am. Chem. Soc.* **2021**, *143*, 8414–8425; b) C. Costentin, S. Drouet, M. Robert, J.-M. Savéant, *Science* **2012**, *338*, 90–94; c) C. Costentin, G. Passard, M. Robert, J.-M. Savéant, *J. Am. Chem. Soc.* **2014**, *136*, 11821–11829.

[25] Y. Tamaki, K. Koike, T. Morimoto, Y. Yamazaki, O. Ishitani, *Inorg. Chem.* **2013**, *52*, 11902–11909.

[26] a) S. Wallin, J. Davidsson, J. Modin, L. Hammarström, *J. Phys. Chem. A* **2005**, *109*, 4697–4704; b) C. K. Prier, D. A. Rankic, D. W. C. MacMillan, *Chem. Rev.* **2013**, *113*, 5322–5363.

[27] Y. Hu, F. Zhan, Q. Wang, Y. Sun, C. Yu, X. Zhao, H. Wang, R. Long, G. Zhang, C. Gao, W. Zhang, J. Jiang, Y. Tao, Y. Xiong, *J. Am. Chem. Soc.* **2020**, *142*, 5618–5626.

[28] X.-Q. Zhu, M.-T. Zhang, A. Yu, C.-H. Wang, J.-P. Cheng, *J. Am. Chem. Soc.* **2008**, *130*, 2501–2516.

[29] E. C. Constable, A. C. King, P. R. Raithby, *Polyhedron* **1998**, *17*, 4275–4289.

[30] F. Teplý, *Collect. Czech. Chem. Commun.* **2011**, *76*, 859–917.

[31] Y. Yamazaki, H. Takeda, O. Ishitani, *J. Photochem. Photobiol. C* **2015**, *25*, 106–137.

[32] M. E. K. Wahba, N. El-Enany, F. Belal, *Anal. Methods* **2015**, *7*, 10445–10451.

[33] M. F. Kuehnel, K. L. Orchard, K. E. Dalle, E. Reisner, *J. Am. Chem. Soc.* **2017**, *139*, 7217–7223.

[34] C. Herrero, A. Quaranta, S. El Ghachtouli, B. Vauzeilles, W. Leibl, A. Aukauloo, *Phys. Chem. Chem. Phys.* **2014**, *16*, 12067–12072.

[35] N. Komatsuzaki, Y. Himeda, T. Hirose, H. Sugihara, K. Kasuga, *Bull. Chem. Soc. Jpn.* **1999**, *72*, 725–731.

[36] X.-C. Nie, R. Hu, R. Liu, A.-X. Zhu, F.-Y. Liu, Q.-Q. Xu, Z. Yang, *Catal. Commun.* **2020**, *134*, 105681.

[37] C. A. Craig, L. O. Spreer, J. W. Otvos, M. Calvin, *J. Phys. Chem.* **1990**, *94*, 7957–7960.
[38] K. Mochizuki, S. Manaka, I. Takeda, T. Kondo, *Inorg. Chem.* **1996**, *35*, 5132–5136.
[39] Q.-Q. Xu, R. Liu, W.-H. Mu, R. Chen, B. Huang, Z. Yang, J.-F. Kou, *Inorg. Chem. Commun.* **2020**, *122*, 108269.
[40] K. Chair, C. A. Luna Caceres, S. Rajak, O. Schott, G. E. Ramírez-Caballero, T. Maris, G. S. Hanan, A. Duong, *ACS Appl. Energ. Mater.* **2022**, *5*, 11077–11090.
[41] M. Bonchio, J. Bonin, O. Ishitani, T–B. Lu, T. Morikawa, A. J. Morris, E. Reisner, D. Sarkar, F. M. Toma, M. Robert, *Nat. Catal.* **2023**, *6*, 657–665.

Manuscript received: December 16, 2023
Revised manuscript received: January 17, 2024
Accepted manuscript online: February 7, 2024
Version of record online: February 27, 2024